Neural, Parallel & Scientific Computations 15 (2007) 165-180

NUMERICAL INVESTIGATION OF LINEAR AND NONLINEAR PHOTOTHERMAL RADIOMETRY ON SILICON WAFERS USING A CHEBYSHEV SPECTRAL METHOD

N. C. PAPANICOLAOU[1], M. NESTOROS[2], AND C. CHRISTOFIDES[3]

[1]Department of Computer Science,
INTERCOLLEGE, P.O. Box 24005, 1700 Nicosia, Cyprus.
papanicolaou.n@intercollege.ac.cy
[2]Department of Engineering,
INTERCOLLEGE, P.O. Box 24005, 1700 Nicosia, Cyprus
[3]Department of Physics,
University of Cyprus, P.O. Box 20537, 1678 Nicosia, Cyprus

ABSTRACT. In the present work we examine the Photothermal Radiometric (PTR) Signal from silicon wafers subject to a modulated light source. The stationary one-dimensional equations are solved numerically using a Galerkin Spectral Method. Shifted Chebyshev Polynomials are used as basis functions and the mixed boundary conditions are imposed via bordering. The scheme's overall convergence and accuracy are verified. Both the linear and nonlinear models are considered and the results confirm the predictions of the physical theory, regarding the dependence of the PTR signal on the governing parameters.

Keywords: spectral methods, shifted Chebyshev polynomials, photothermal radiometry.

MSC 2000 Subject Classification: 37L65, 74S25, 65L10, 65L20, 78A40.

1. INTRODUCTION.

Since the early 1980's, several photothermal techniques have been developed for the characterization of different classes of materials, ranging from biological samples to solar cells, as well as for imaging of subsurface defects in metal lines, and implanted semiconductor wafers. The contactless and non-destructive character of photothermal techniques is their main advantage over other traditional methods of characterization and has made some of the photothermal techniques very popular in the semiconductor industry.

Photothermal radiometry (PTR) [2] is based on the detection of the blackbody radiation emitted from a material excited by a modulated light source and it is shown to be extremely sensitive [3] to the electronic properties of semiconductors and more specifically: carrier lifetime, and electron diffusivity.

Received February 1, 2007

When a semiconductor is illuminated with super bandgap light of photon energy, $h\nu$, electrons in the valence band absorb the incident energy and cross the forbidden energy gap (E_g) towards the conduction band, leaving an equal number of holes behind in the valence band. On a picosecond time scale electrons and free carriers become thermalised with the lattice through phonon interaction, releasing the excess energy $h\nu - E_g$, and lie on the bottom of conduction band (electrons) and top of the valence band (holes). In indirect band gap semiconductors like silicon, electrons and holes diffuse for a short time known as carrier lifetime τ_{eff}, before they recombine via non-radiative process releasing energy E_g, to the lattice.

When the illumination of the semiconductor is harmonically modulated, wavelike solutions to the electronic carrier's diffusion equation (2.1) and heat diffusion equation (2.2) exist. These solutions are known as free carrier waves and thermal waves respectively. Thermalization and recombination result in the rise of the local temperature of the semiconductor and a consequent modification of Planck's distribution, resulting in a modulated blackbody emission. The photoexcited free carriers consist an additional source of infrared radiation because they increase the infrared absorption of the semiconductor. The reason is that according to Kirchhoff's Law of detailed balance the rate of emission of black body radiation per wavelength interval at equilibrium with its surroundings is equal to the rate of absorption of incident radiation for the same wavelength interval.

In this work we develop a fast and accurate Galerkin type spectral method, to investigate various aspects of the linear model such as the dependence of the PTR signal on the modulation frequency of the excitation beam and the free carrier lifetime. In addition, the effect of the non-linearity on the solutions of the heat and free carrier diffusion equations is examined. This study of the PTR signal dependence on the physical parameters requires many runs of the numerical code, which makes an efficient algorithm a necessity.

2. THE GOVERNING EQUATIONS.

2.1. Simplifications.

The PTR (Photothermal Radiometric) signal in semiconductors can be divided into two main contributions, depending on the local variations of temperature ΔT and free carrier concentration ΔN. In order to obtain the PTR signal we must first solve the plasma and thermal diffusion equations for an isotropic medium, which in their full dimensional form read [4]:

$$\frac{\partial(\Delta N)}{\partial t} = D_N \nabla^2(\Delta N) - \frac{\Delta N}{\tau_{eff}} + \frac{\partial n_0}{\partial T}\frac{\Delta T}{\tau_{eff}} + \Phi\,\psi_p(r)\,\alpha\,\mathrm{e}^{-\alpha z}\,\mathrm{e}^{\mathrm{i}\omega t}, \tag{2.1}$$

$$\frac{\partial(\Delta T)}{\partial t} = D_T \nabla^2(\Delta T) + D_T \frac{E_g}{\kappa} \frac{\Delta N}{\tau_{eff}} + D_T \frac{h\nu - E_g}{\kappa} \Phi \psi_p(r) \alpha \mathrm{e}^{-\alpha z} \mathrm{e}^{\mathrm{i}\omega t} \tag{2.2}$$

subject to the boundary conditions

$$D_N \frac{\partial(\Delta N)}{\partial z}\Big|_{z=0} = S_1 \cdot \Delta N(z=0) \quad , \quad -D_N \frac{\partial(\Delta N)}{\partial z}\Big|_{z=L} = S_2 \cdot \Delta N(z=L) \tag{2.3}$$

and

$$\kappa \frac{\partial(\Delta T)}{\partial z}\Big|_{z=0} = S_1 E_g \cdot \Delta N(z=0) \quad , \quad -\kappa \frac{\partial(\Delta T)}{\partial z}\Big|_{z=L} = S_2 E_g \cdot \Delta N(z=L), \tag{2.4}$$

where $D_N = 24 \cdot 10^{-4} m^2/s$ and $D_T = 9 \cdot 10^{-5} m^2/s$ are the ambipolar electron diffusivity and thermal diffusivity respectively; n_0 is the equilibrium free-carrier density, ω is the angular frequency ($\omega = 2\pi f$, where f is the modulation frequency of the excitation beam), $\kappa = 140 W/mK$ is the thermal conductivity, $E_g = 1.79 \cdot 10^{-19} J$ is the band gap energy, $h\nu = 3.86 \cdot 10^{-19} J$ is the photon energy of the pump beam, t is time and $\alpha = 3 \cdot 10^6 m^{-1}$ the optical absorption coefficient of the sample. Φ is the incident photon flux which is given by $\Phi = \dfrac{P \cdot (1-R)}{h\nu \pi d^2}$, where P is the incident light power, $R = 0.3$ the reflectivity of the material at the excitation wavelength, $d = 10^{-4} m$ the excitation beam radius and $\Psi_p(r) = \exp(-2r^2/d^2)$ is the Gaussian profile of the beam intensity. $L = 2 \cdot 10^{-3} m$, is the thickness of the silicon wafer.

The quantity τ_{eff} is the effective recombination lifetime of the free carriers, and is given by

$$\frac{1}{\tau_{eff}} = \frac{1}{\tau} + \gamma^* |\Delta N|^2. \tag{2.5}$$

The constant term τ is the recombination lifetime due to the so-called Shockley-Read-Hall recombination mode which is independent of the free carrier concentration. The nonlinear term is due to Auger recombination [5, 6]. This is a three particle interaction where a conduction band electron and a valence band hole recombine and the excess energy is given to a third particle, electron or hole. The Auger mode occurs at elevated free carrier injection levels and its lifetime is given by $\tau_{Auger} = 1/(\gamma^* |\Delta N|^2)$ (complex formulation). The parameter $\gamma^* = 3.88 \cdot 10^{-43} m^6 s^{-1}$ combined with the characteristic magnitude of ΔN describes the relative impact of the nonlinear term.

The total PTR signal is given by the relation

$$S_{PTR} = S_N + S_T, \quad \text{where} \quad S_N = C_N \int_0^L \Delta N \mathrm{d}z \quad \text{and} \quad S_T = C_T \int_0^L \Delta T \mathrm{d}z \tag{2.6}$$

are the total free carrier and thermal contributions respectively, and the free carrier and thermal coefficients have values $C_N = 1$, $C_T = 10^{23}$ for the purposes of this work.

Solving the full form of the governing equations poses an extremely difficult task, so we take advantage of various physical assumptions and focus just on certain subcases of the model. When working at relatively low temperatures thermal activation, (the third term in the r.h.s. of (2.1)) can be ignored, effectively decoupling our equations.

Under the assumption that the free carriers recombine almost instantaneously after the excitation beam is stopped, the temporal dependence of the free carrier density is negligible. In addition, assuming that the excitation beam radius is of the order of mm, which is much greater than the thermal and free carrier wavelengths in silicon, the thermal and free carrier waves propagate only in one dimension (z-direction) [7].

Hence, the dimensional 1-D equations for the quasi-stationary vibrations are

$$\frac{\mathrm{d}^2 N^*}{\mathrm{d}z^{*^2}} - \frac{1 + \mathrm{i}\omega^* \tau}{D_N \tau} N^* = -\frac{\alpha^* P(1-R)}{h\nu \pi d^2 D_N} \mathrm{e}^{-\alpha^* z^*} + \frac{\gamma^*}{D_N} |N^*|^2 N^* \tag{2.7}$$

$$\frac{\mathrm{d}^2 T^*}{\mathrm{d}z^{*^2}} - \frac{\mathrm{i}\omega^*}{D_T} T^* + \frac{E_g}{\kappa \tau} N^* = -\frac{\alpha^* P(1-R)(h\nu - E_g)}{h\nu \kappa \pi d^2} \mathrm{e}^{-\alpha^* z^*} + \gamma^* \frac{E_g}{\kappa} |N^*|^2 N^*, \tag{2.8}$$

where $\Delta N = N^*(z^*) e^{i\omega t}$, $\Delta T = T^*(z^*) e^{i\omega t}$ and the * denotes dimensional variables.

The boundary conditions are of the third kind (Robin conditions):

$$D_N \frac{\mathrm{d}N^*}{\mathrm{d}z^*}\Big|_{z^*=0} = S_1^* N^*(0) \quad \text{and} \quad D_N \frac{\mathrm{d}N^*}{\mathrm{d}z^*}\Big|_{z^*=L} = -S_2^* N^*(L) \tag{2.9}$$

$$-\kappa \frac{\mathrm{d}T^*}{\mathrm{d}z^*}\Big|_{z^*=0} = S_1^* E_g N^*(0) \quad \text{and} \quad \kappa \frac{\mathrm{d}T^*}{\mathrm{d}z^*}\Big|_{z^*=L} = S_2^* E_g N^*(L). \tag{2.10}$$

2.2. **Nondimensionalization.**

Dimensionless variables are introduced according to the scheme

$$N^* = \hat{N} N, \; T^* = \hat{T} T, \; z^* = L z, \; \frac{\mathrm{d}}{\mathrm{d}z^*} = \frac{1}{L} \frac{\mathrm{d}}{\mathrm{d}z}, \tag{2.11}$$

where $L = 2 \cdot 10^{-3} m$, $\hat{N} = 10^{22} m^{-3}$, $\hat{T} = 0.1K$. The values for $\hat{N}$ and $\hat{T}$ have been selected using typical values of the dimensional solutions N^* and T^*. This leads to the dimensionless equations

$$\frac{\mathrm{d}^2 N}{\mathrm{d}z^2} - \delta(1 + \mathrm{i}\Omega) N = -\lambda \mathrm{e}^{-\alpha z} + \gamma |N|^2 N, \tag{2.12}$$

$$\frac{\mathrm{d}^2 T}{\mathrm{d}z^2} - (\mathrm{i}\Omega \delta_T)\, T + \beta N = -\lambda_T \mathrm{e}^{-\alpha z} + \mu |N|^2 N, \tag{2.13}$$

and the dimensionless boundary conditions:

$$\frac{\mathrm{d}N}{\mathrm{d}z}\Big|_{z=0} = s_1 N(0) \quad , \quad \frac{\mathrm{d}N}{\mathrm{d}z}\Big|_{z=1} = -s_2 N(1), \tag{2.14}$$

$$-\frac{\mathrm{d}T}{\mathrm{d}z}\Big|_{z=0} = s_3 N(0) \quad , \quad \frac{\mathrm{d}T}{\mathrm{d}z}\Big|_{z=1} = s_4 N(1). \tag{2.15}$$

The dimensionless parameters are given by

$$\alpha = \alpha^* L = 6 \cdot 10^3, \ \delta = \frac{L^2}{D_n \tau}, \ \delta_T = \frac{L^2}{\tau D_T}, \ \beta = \frac{E_g L^2 \hat{N}}{\kappa \tau \hat{T}},$$

$$\lambda = \frac{\alpha^* P L^2 \hat{N}^{-1}}{h\nu\pi d^2 D_N} = \frac{3.24}{\pi} \cdot 10^6, \ \lambda_T = \frac{\alpha^* P L^2 (h\nu - E_g)}{\hat{T} h\nu\pi D^2 \kappa} = \frac{6.21}{3.86 \cdot 14\pi} \cdot 10^7$$

$$s_1 = \frac{L S_1^*}{D_N} = \frac{10}{12}, \ s_2 = \frac{L S_2^*}{D_N} = \frac{1}{12}, \ s_3 = \frac{S_1^* E_g \hat{N} L}{\kappa \hat{T}} = \frac{3.58}{14}$$

$$s_4 = \frac{S_2^* E_g \hat{N} L}{\kappa \hat{T}} = \frac{0.358}{14}.$$

Considering that usually $\tau \in [10^{-6}, 10^{-4}]$ we have the following range of values: $\delta \in [16.66, 1666.66]$, $\delta_T \in [444.44, 44444.44]$, $\beta \in [5.114, 511.429]$.

There are significant advantages in treating the non-dimensional problem. Firstly, we are able to fully appreciate the effect of the physical parameters on the solutions. Secondly, the magnitude of these parameters is reduced significantly which is useful for computational purposes. And thirdly, the differentiation matrices become independent of L.

At first, we concentrate on the linear model and thus we set $\tau_{eff} = \tau$. This is equivalent to setting $\gamma^* = 0$ in (2.7, 2.8) and $\gamma = \mu = 0$ in (2.12, 2.13).

The dimensionless linear boundary value problem reads

$$\frac{\mathrm{d}^2 N}{\mathrm{d}z^2} - \delta(1 + \mathrm{i}\Omega) N = -\lambda \mathrm{e}^{-\alpha z}, \tag{2.16}$$

$$\frac{\mathrm{d}^2 T}{\mathrm{d}z^2} - (\mathrm{i}\Omega\delta_T)\, T + \beta N = -\lambda_T \mathrm{e}^{-\alpha z}, \tag{2.17}$$

subject to (2.14, 2.15).

It possesses the following analytic solution:

$$N(z) = c_1 \mathrm{e}^{\sigma_N z} + c_2 \mathrm{e}^{-\sigma_N z} + A\mathrm{e}^{-\alpha z}, \tag{2.18}$$

$$T(z) = c_3 \mathrm{e}^{\sigma_T z} + c_4 \mathrm{e}^{-\sigma_T z} + W_1 \mathrm{e}^{\sigma_N z} + W_2 \mathrm{e}^{-\sigma_N z} + W_3 \mathrm{e}^{-\alpha z} \tag{2.19}$$

where,

$$A = \frac{-\lambda}{\alpha^2 - \sigma_N^2},\ W_1 = \frac{-c_1\beta}{\sigma_N^2 - \sigma_T^2},\ W_2 = \frac{-c_2\beta}{\sigma_N^2 - \sigma_T^2},\ W_3 = \frac{-\lambda_T - A\beta}{\alpha^2 - \sigma_T^2},$$

$$c_2 = \frac{A\left[e^{-\alpha}(\alpha - s_2)(\sigma_N - s_1) - e^{\sigma_N}(\alpha + s_1)(\sigma_N + s_2)\right]}{e^{\sigma_N}(s_1 + \sigma_N)(s_2 + \sigma_N) + e^{-\sigma_N}(s_2 - \sigma_N)(\sigma_N - s_1)},$$

$$c_1 = \frac{A(\alpha + s_1) + c_2(s_1 + \sigma_N)}{\sigma_N - s_1},$$

$$c_3 = \frac{-W_1\sigma_N e^{\sigma_N} + W_2\sigma_N e^{-\sigma_N} + \alpha W_3 e^{-\alpha} + s_4(c_1 e^{\sigma_N} + c_2 e^{-\sigma_N} + A e^{-\alpha})}{\sigma_T(e^{\sigma^T} - e^{-\sigma^T})}$$
$$+ \frac{-e^{-\sigma_T}\left[(-W_1 + W_2)\sigma_N + \alpha W_3 - s_3(c_1 + c_2 + A)\right]}{\sigma_T(e^{\sigma^T} - e^{-\sigma^T})},$$

$$c_4 = \frac{1}{\sigma_T}\left[c_3\sigma_T + W_1\sigma_N - W_2\sigma_N - \alpha W_3 + s_3(c_1 + c_2 + A)\right].$$

3. THE NUMERICAL METHOD.

3.1. The Orthogonal System of Functions.

The numerical scheme is a Galerkin Spectral Method using shifted Chebyshev Polynomials as basis functions. This choice was made because the problem is set on the finite interval $[0, 1]$ and due to the fact that we also treat the nonlinear model, which contains cubic nonlinear terms. Also, Chebyshev expansions of well-behaved functions are expected to have geometric (or exponential) convergence, a feature that is very important in constructing a fast and accurate scheme.

Chebyshev Polynomials of the first kind are defined by the trigonometric relation

$$T_n(x) = \cos n\theta \quad \text{where} \quad x = \cos\theta. \tag{3.1}$$

They form a system of orthogonal functions on $[-1, 1]$, with respect to the weight function

$$w(x) = \frac{1}{\sqrt{1 - x^2}}. \tag{3.2}$$

The orthogonality relation is:

$$\int_{-1}^{1} \frac{T_i(x)T_j(x)}{\sqrt{1 - x^2}}\mathrm{d}x = \begin{cases} 0 & i \neq j \\ \frac{\pi}{2} & i = j \neq 0 \\ \pi & i = j = 0. \end{cases}$$

The Fourier Series of a function $F(x)$ expanded in the T_n basis is

$$F(x) = \sum_{n=0}^{\infty} f_n T_n(x), \tag{3.3}$$

where the Fourier coefficients are the inner products

$$f_n = < F(x), T_n(x) >_w = \frac{2}{\pi} \int_{-1}^{1} \frac{F(x)T_n(x)}{\sqrt{1-x^2}} \mathrm{d}x \quad \text{for } n \geq 1$$

$$f_0 = < F(x), T_0(x) >_w = \frac{1}{\pi} \int_{-1}^{1} \frac{F(x)T_0(x)}{\sqrt{1-x^2}} \mathrm{d}x \quad \text{for } n = 0.$$

We define the shifted Chebyshev polynomials $T_n^*(x)$ on $[0,1]$ by

$$T_n^*(x) = T_n(2x-1), \tag{3.4}$$

where $T_n(x)$ denotes the usual Chebyshev polynomials. As expected, the T_n^* form an orthogonal system on $[0,1]$, but with respect to the translated weight function

$$w^*(x) = w(2x-1) = \frac{1}{\sqrt{1-(2x-1)^2}}. \tag{3.5}$$

The orthogonality relation becomes

$$\int_0^1 \frac{2\,T_i^*(x)T_j^*(x)}{\sqrt{1-(2x-1)^2}} \mathrm{d}x = \begin{cases} 0 & i \neq j \\ \frac{\pi}{2} & i = j \neq 0 \\ \pi & i = j = 0. \end{cases}$$

The Fourier Series of a function $F(x)$ expanded in the T_n^* basis is

$$F(x) = \sum_{n=0}^{\infty} f_n T_n^*(x), \tag{3.6}$$

where the Fourier coefficients are the inner products

$$f_n = < F(x), T_n^*(x) >_{w^*} = \frac{2}{\pi} \int_0^1 \frac{2\,F(x)T_n^*(x)}{\sqrt{1-(2x-1)^2}} \mathrm{d}x \quad \text{for } n \geq 1$$

$$f_0 = < F(x), T_0^*(x) >_{w^*} = \frac{1}{\pi} \int_0^1 \frac{2\,F(x)T_0^*(x)}{\sqrt{1-(2x-1)^2}} \mathrm{d}x \quad \text{for } n = 0.$$

The appropriate formulas for expanding the derivatives of the T_n^* into a linear combination of T_i^* are

(3.7)

$$T_n^{*''}(x) = \sum_{i=0}^{n} \chi_{ni} T_i^*(x) \quad \text{where} \quad \chi_{ni} = \begin{cases} 4n(n^2-i^2)c_i, & n+i \text{ even} \\ 0, & n+i \text{ odd}; \end{cases}$$

$$T_n^{*'}(x) = \sum_{i=0}^{n} v_{ni} T_i^*(x) \quad \text{where} \quad v_{ni} = \begin{cases} 4nc_i, & n+i \text{ odd} \\ 0, & n+i \text{ even}; \end{cases} \tag{3.8}$$

and $c_i = 1$ for $i = 1, \ldots, n$ and $c_0 = \frac{1}{2}$. They are easily derived in exactly the same manner as their counterparts for the regular T_n functions, except that for each derivative there is a multiplication by a factor of 2.

The product formula

$$T_i^*(x)T_j^*(x) = \frac{1}{2}\left[T_{i-j}^* + T_{i+j}^*\right] \tag{3.9}$$

is a direct consequence of the trigonometric definition of T_n^*,

$$T_n^*(x) = \cos n\theta \quad \text{where} \quad 2x - 1 = \cos\theta. \tag{3.10}$$

It is essential for the treatment of the nonlinear term, as will be seen in subsection 4.2.

3.2. **Derivation of the Galerkin Equations.**

In order for us to obtain the Galerkin Equations we develop the sought functions into spectral series with respect to $T_n^*(z)$:

$$N(z) = \sum_{i=0}^{I} a_i T_i^*(z) \quad , \quad T(z) = \sum_{i=0}^{I} b_i T_i^*(z), \tag{3.11}$$

where the unknown coefficients a_i and b_i are complex-valued. We prefer to work in the complex domain because separating the sought functions into real and imaginary parts

$$N(z) = N_{Re}(z) + \mathrm{i}N_{Im}(z) \quad , \quad T(z) = T_{Re}(z) + \mathrm{i}T_{Im}(z)$$

and developing them into series would have led to a coupled system.

We introduce series (3.11) into Eqns. (2.16, 2.17), multiply all terms by the test functions $T_j^*(z)$, $j = 0, 1, 2, \ldots, I$ and integrate over $[0, 1]$. Making use of the orthogonality of the $T_n^*(z)$ functions, simplifying the constants $\pi/2$ for $j = 1, 2, \ldots I$ and π for $j = 0$ respectively and utilizing the formulas compiled in the previous subsection, we obtain the following linear algebraic systems of $I + 1$ equations with $I + 1$ unknowns for the coefficients a_i and b_i:

$$\sum_{i=0}^{I} \chi_{ij} a_i - \sigma_N^2 a_j = -\lambda f_j, \qquad \text{where } \sigma_N^2 = \delta(1 + \mathrm{i}\Omega) \tag{3.12}$$

$$\sum_{i=0}^{I} \chi_{ij} b_i - \sigma_T^2 b_j = -\lambda_T f_j - \beta a_j, \qquad \text{where } \sigma_T^2 = \mathrm{i}\Omega\delta_T. \tag{3.13}$$

We consider the above as two separate systems because (3.12) can be solved first and then the obtained values of the a_i may be substituted into (3.13).

The vector f_j is due to the Galerkin expansion of the function $e^{-\alpha z}$ and is defined by

$$f_j = \int_0^1 \frac{2e^{-\alpha z} T_j^*(z)}{1-(2z-1)^2} dz \quad , \quad j = 0, 1, 2, \ldots, I \tag{3.14}$$

Utilizing the substitution $\cos\theta = 2z - 1$ and (3.10) we obtain

$$f_j = \int_0^1 \frac{2e^{-\alpha z} T_j^*(z)}{1-(2z-1)^2} dz = \int_0^\pi e^{-\frac{\alpha}{2}(1+\cos\theta)} \cos(j\theta) d\theta \quad , \quad j = 0, 1, 2, \ldots, I$$

We then evaluate the trigonometric integral using the trapezoidal rule. The reason for this is that due to the periodic integrand the trapezoidal rule converges faster than any power of h, where h is the distance between two consecutive integration nodes (see [8]). Furthermore, we avoid any difficulties that may arise due to the singularities observed in the original integral.

The boundary conditions (2.14, 2.15) are imposed via bordering (see [9]), i.e. the last two rows of the matrices and r.h.s. vectors in (3.12) and (3.13) are replaced by

$$\left[s_1(-1)^j - \sum_{i=0}^{I} v_{ij}(-1)^i \right] a_j = 0 \ , \qquad - \left[s_2 - \sum_{i=0}^{I} v_{ij} \right] a_j = 0 \tag{3.15}$$

and

$$\sum_{j=0}^{I} \left(\sum_{i=0}^{I} v_{ji}(-1)^i \right) b_j = s_3 \sum_{j=0}^{I} (-1)^j a_j \ , \qquad \sum_{j=0}^{I} \left(\sum_{i=0}^{I} v_{ji} \right) b_j = s_4 \sum_{j=0}^{I} a_j . \tag{3.16}$$

When the boundary conditions are implemented as we have just described, the technique is called the tau method in some of the literature ([10]). Despite the fact that this destroys the triangularity of the matrices, it improves their condition numbers.

The two linear systems we have obtained are complex-valued. The matrices are inverted with the aid of the IMSL routine DLINCG.

4. THE NUMERICAL RESULTS.

4.1. The Linear Model.

The scheme's overall accuracy is verified by comparing the numerical solution to the analytic solution (2.18),(2.19) of the linear system. The case demonstrated in Fig. 1 is $P = 0.025W$, $\tau = 10^{-5}s$, $f = 100Hz$. The modulus of the absolute error does not exceed 0.1% for the free carrier concentration N and 0.0000001% for the temperature T.

The following figure shows the convergence rate of our scheme for the same case. This is found to be geometric as predicted by the theory of

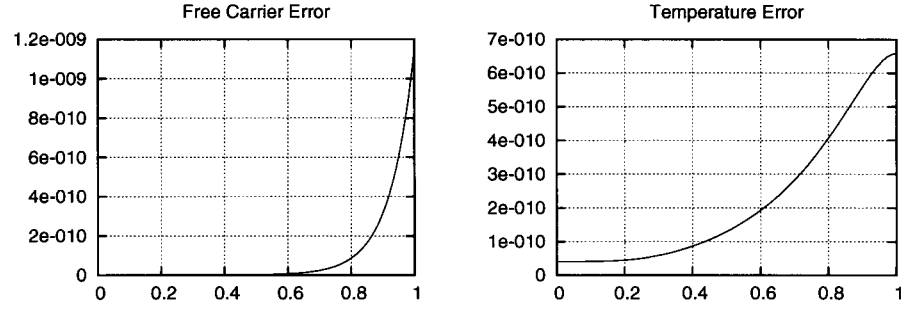

FIGURE 1. Modulus of absolute error in solving the linear system. Left panel: free carrier diffusion; Right panel: temperature.

Chebyshev spectral series. The decay of the coefficients 380-400 is supergeometric, until the order of the round-off error is reached.

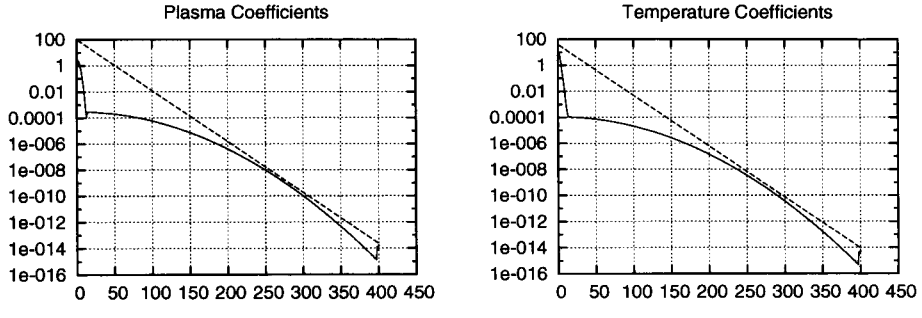

FIGURE 2. Convergence of the spectral series. Left panel: solid line: $|a_j|$, dashed line: the best fit curve $|a_j| = 100\exp(-0.09j)$; Right panel: solid line: $|b_j|$, dashed line: the best fit curve $|b_j| = 40\exp(-0.09i)$.

The calculated behavior of the PTR signal amplitude vs the frequency (see Fig. 3) is in very good agreement with the predictions of the theory. All the characteristic features of the thermal wave contribution ($1/f$ dependence) at lower frequencies, then the plateau of free carrier dominance and finally the free carrier diffusion regime initiated at the frequency where $2\pi f\tau \approx 1$ are evident in the graphs for two different values of carrier lifetime.

The PTR phase difference of the thermal wave contribution is independent from the modulation frequency and is always at $-90°$ relative to excitation, while the phase of the free carriers depends on the modulation frequency f. The free carriers are in phase with the excitation at low frequencies ($2\pi f < \tau$) and as the modulation frequency is increasing their phase moves towards $-90°$. In Fig. 4 the phase of the PTR signal is presented as

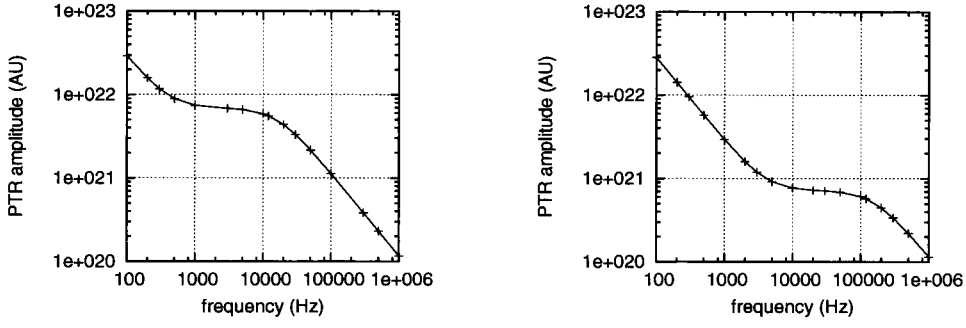

FIGURE 3. PTR signal amplitude dependence on frequency f. Note the characteristic bend at $f \approx \frac{1}{2\pi\tau}$. Left panel: $\tau = 10^{-5}s$; Right panel: $\tau = 10^{-6}s$.

a function of the modulation frequency for two values of the carrier lifetime; $\tau = 10^{-5}s$ and $\tau = 10^{-6}s$. For small values of modulation frequency the thermal contribution is stronger than the free carrier one and hence the phase is at $-90°$. As the modulation frequency is increasing above $100Hz$ the free carrier contribution is dominating the signal and the phase is moving towards $0°$. For the case of longer lifetime this transition from $-90°$ to $0°$ happens earlier than the case of shorter lifetime. At higher frequencies the phase of the signal (dominated from the free carriers) is moving back to $-90°$ and for the case of the longer lifetime this happens earlier compared to the short lifetime.

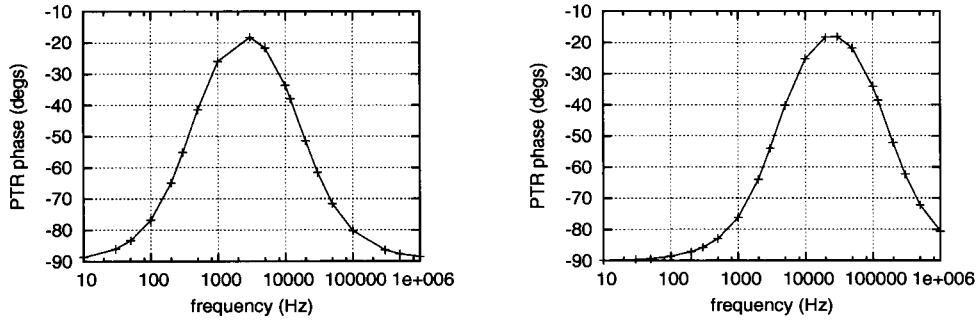

FIGURE 4. PTR signal phase dependence on frequency f. Note the shift of the peak (area of free carrier dominance). Left panel: $\tau = 10^{-5}s$; Right panel: $\tau = 10^{-6}s$.

4.2. **The Nonlinear Model .** The dimensional 1-D equations for the nonlinear case are (2.7, 2.8) subject to the boundary conditions (2.9, 2.10). It may seem that with γ^* having such a small value, the nonlinearity can always be disregarded. However, this is not the case since a typical value (see

subsection 2.2) for the dimensional solution N^* is of order 10^{22} and thus $\gamma^*|N^*|^2N^* \approx O\left(10^{23}\right) \approx N^*$.

Recall that the respective nondimensional boundary value problem is given by (2.12, 2.13), where $\gamma = \frac{\gamma^* L^2 \hat{N}^2}{D_N} = 1.552$, $\mu = \frac{\gamma^* E_g L^2 \hat{N}^3}{\kappa \hat{T}} \approx 0.0198$ and the boundary conditions are given by (2.14, 2.15). The values of these dimensionless parameters clearly demonstrate the significance of the nonlinearity for the aforementioned values of N^*.

Following the same procedure as for the linear case (cf. Section 3) we arrive at

$$(4.1)\quad \sum_{i=0}^{I} \chi_{ij} a_i - \sigma_N^2 a_j = -\lambda f_j + \gamma \sum_{i=0}^{I} \sum_{k=0}^{I} \frac{1}{2} s_i a_k (\delta_{i+k,j} + \delta_{|i-k|,j})$$

$$(4.2)\quad \sum_{i=0}^{I} \chi_{ij} b_i - \sigma_T^2 b_j = -\lambda_T f_j - \beta a_j - \mu \sum_{i=0}^{I} \sum_{k=0}^{I} \frac{1}{2} s_i a_k (\delta_{i+k,j} + \delta_{|i-k|,j})$$

where $\sigma_N^2 = \delta(1 + \mathrm{i}\Omega)$ and $\sigma_T^2 = \mathrm{i}\Omega\delta_T$.

The term $s_i = \frac{1}{2} \sum_{l=0}^{I} \sum_{m=0}^{I} \bar{a}_l a_m (\delta_{l+m,i} + \delta_{|l-m|,i})$ originates from the inner product $< |N(z)|^2, T_i^*(z) >_{w^*} = < N\bar{N}, T_i^*(z) >_{w^*}$. The terms s_i and the double sums in the r.h.s of (4.1) and (4.2) are due to the representation of the nonlinear term and are obtained with the aid of (3.9).

Again, to impose the boundary conditions bordering is utilized and the last two equations in systems (4.1) and (4.2) are replaced by (3.15) and (3.16) respectively. The resulting algebraic system for $\boldsymbol{a} = \{a_j\}_{j=0}^{I}$ may be written in matrix form as

$$(4.3)\quad \mathsf{W}\,\boldsymbol{a} = \boldsymbol{f} + \boldsymbol{g}$$

where g denotes the nonlinear term. It is solved following a semi-implicit scheme and simple iterations, i.e.

$$(4.4)\quad \boldsymbol{a}^{[n+1]} = \theta \mathsf{W}^{-1} \left(\boldsymbol{f} + \boldsymbol{g}^{[n]} \right) + (1 - \theta) \boldsymbol{a}^{[n]}$$

The relaxation parameter θ which assumes values $0 < \theta \leq 1$ is especially useful for the convergence of the simple iterations in the upper range of the modulation frequency values. Note that the matrix is only inverted once before the beginning of the simple iterations which is very important for the efficiency of the scheme.

Since there is no exact analytic solution of the nonlinear dynamical system (2.12), (2.13) is known, the assessment of the nonlinear approximation (4.1), (4.2) is limited to (i) verifying the convergence rate of the Galerkin spectral series; and (ii) examining whether the predictions of the physical theory (PhotoThermal Radiometry) are mirrored in the numerical calculations.

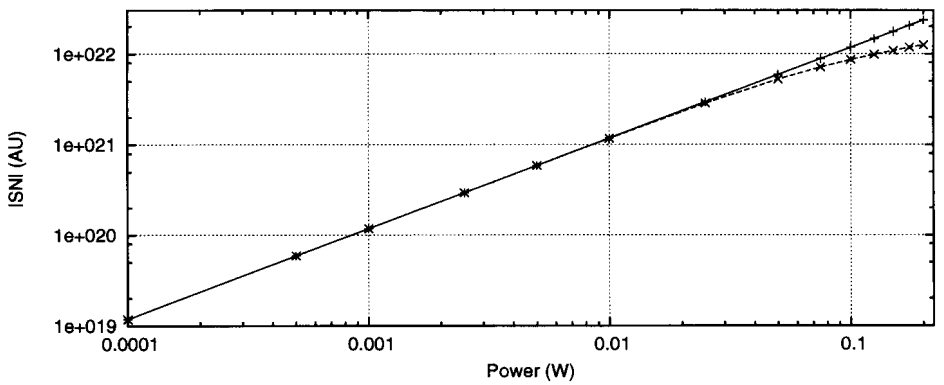

FIGURE 5. Total free carrier contribution amplitude $|S_N|$ as a function of power. Solid line: linear. **D**ashed line: nonlinear.

Fig. 5 depicts the dependence of the total free carrier contribution $S_N = \int_0^1 N^*(z)\mathrm{d}z$ as a function of power. The nonlinear behavior is already evident at incident power $0.01W$ (corresponding to an energy flux of 31.8 W/cm^2). As incident flux is increased, a higher population of free carriers is generated. This results in a decrease of free carrier lifetime (see Eqn. 2.5) and consequently the free carrier population is less than the one predicted by the linear model.

In Fig. 6 we demonstrate the exponential convergence rate of the spectral series coefficients for $P = 0.1W$, $\tau = 5{\cdot}10^{-6}s$, $f = 4000Hz$, $D_N = 10^{-4}$, parameter values for which their is a pronounced nonlinear effect (see Fig. 5).

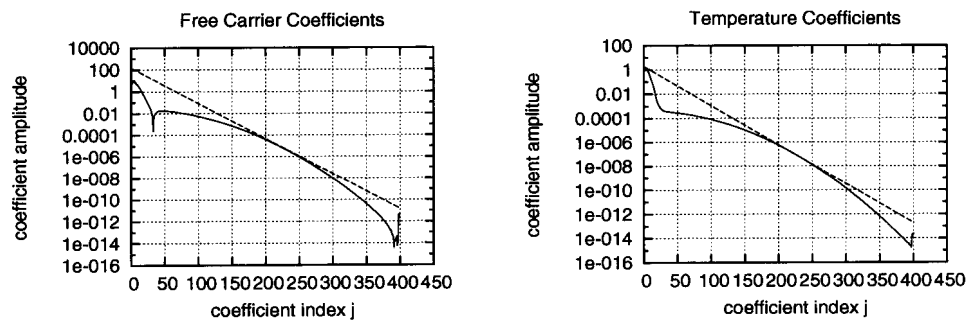

FIGURE 6. Left panel: Convergence of the spectral series for the free carriers. Solid line: $|a_j|$, dashed line: the best fit curve $|a_j| = 150\exp(-0.075j)$. Right panel: Convergence of the spectral series for the temperature. Solid line: $|b_j|$, dashed line: the best fit curve $|b_j| = 2\exp(-0.075j)$.

The free carrier density at the surface of the sample $N(0)$ is yet another quantity of physical and mathematical importance for our comparison of the linear and nonlinear models. A simulation of the free carrier density at the surface of the sample is shown in Fig. 7 as a function of the modulation frequency, for both the linear and non-linear cases. The value of the excitation power used is $P = 0.1W$ that lies beyond the value that defines the transition to the non-linear regime as we have already established.

Fig. 7 presents two important features. The first is the decreased value of the amplitude corresponding to the non-linear model relative to the linear one, something that is evident from Fig. 5. The other important feature is the shift of the characteristic frequency at which the slope changes, towards higher values. The fact that the characteristic frequency is inversely proportional to the carrier lifetime is in accordance to the decrease of carrier lifetime due to the Auger recombination mechanism, whose importance is dictated from the excitation power increase. The phenomenon of frequency shift towards higher values is even more evident in the free carrier density phase graph. The resolution of phase is in general higher in all photothermal experiments.

For high values of modulation frequency we observe that the linear and non linear model converge, since the variation of both amplitude and phase depends mostly on the electronic diffusivity and surface recombination velocity, parameters that are the same in both cases.

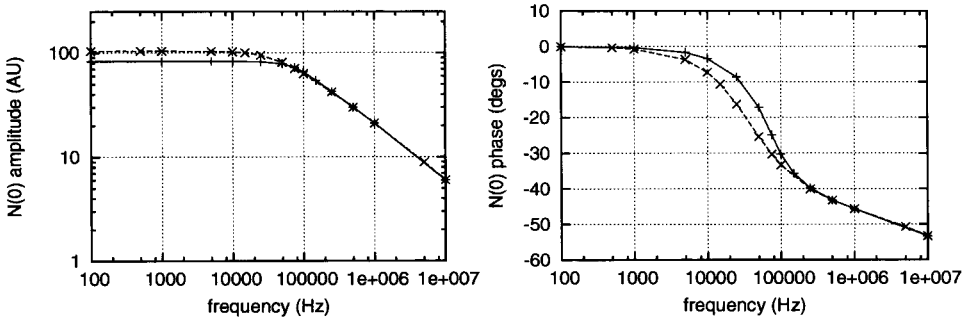

FIGURE 7. Left panel: Amplitude $|N(0)|$ as a function of frequency. Right panel: Phase of surface free carriers. Solid line: nonlinear, dashed line: linear.

5. CONCLUSIONS.

In the present work, a Galerkin type spectral scheme is constructed for the numerical investigation of the PhotoThermal Radiometric Signal from silicon wafers subject to a modulated light source. Following physical assumptions, the full time-dependent 2-D system of PDEs is reduced to a dynamical system and the obtained equations are nondimensionalized.

Shifted Chebyshev polynomials are used as basis functions and the boundary conditions are imposed via bordering. The convergence rate of the method for both the linear and nonlinear systems is found to be exponential. The spectral solution is found to be in good agreement with the available exact analytic solution of the linear model.

The results obtained for both the linear and nonlinear models match the predictions of Photothermal Radiometry theory. Firstly, for the linear model, the PTR amplitude and phase dependence on the modulation frequency clearly have the expected bend and peak respectively at the characteristic frequency value $f \approx \frac{1}{2\pi\tau}$. Secondly, for the nonlinear model, we have the expected decrease in free carrier population and shift of the characteristic frequency compared to the linear case.

Thus, we have constructed and tested an efficient and accurate method which can also be used for multilayer heterostructures.

Acknowledgement. The authors would like to thank Dr. C. I. Christov of the Mathematics Department of the University of Louisiana at Lafayette for his many valuable suggestions.

REFERENCES

[1] N. C. Papanicolaou, M. Nestoros, and C. Christofides. Numerical simulation of nonlinear photothermal radiometry on silicon wafers using a Chebyshev Galerkin method. In *Proceedings of Neural, Parallel, and Scientific Computations*, volume 3, pages 188–192, USA, 2006. Dynamic Publishers Inc.

[2] C. Christofides, M. Nestoros, and A. Othonos. Photothermal radiometric study of implanted semiconductors. In A. Mandelis and P. Hess, editors, *Progress in Photothermal and Photoacoustic Science and Technology*, volume IV, chapter 4. Bellingham, USA, 2000.

[3] M. E. Rodriguez, J. A. Garcia, and A. Mandelis. Infrared photothermal radiometry investigation of deep subsurface defects in semiconductor materials. *Rev. Scient. Instr.*, 74(1):839–841, 2003.

[4] C. Christofides. Photothermal thermoreflectance investigation of implanted wafers. annealing kinetics of defects. In C. Christofides and G. Ghibaudo, editors, *Effect of Disorder and Defects in Ion-Implanted Semiconductors: Optical and Photothermal Characterization, Semiconductors and Semimetals*, volume 46, chapter 4. Academic Press, USA, 1997.

[5] M. J. Kerr and A. Cuevas. General parametrization of Auger recombination in crystalline silicon. *J. Appl. Phys.*, 91(4):2473–2480, 2002.

[6] B. C. Forget and D. Fournier. Auger recombination in modulated photoreflectance characterization of silicon wafers. *Appl. Phys. Lett.*, 61(19):2341–2343, 1992.

[7] A. Othonos, C. Christofides, and A. Mandelis. Photothermal radiometric investigation of implanted silicon: The influence of dose and thermal annealing. *Appl. Phys. Lett.*, 69(6):821–823, 1996.

[8] K. E. Atkinson. *An Introduction to Numerical Analysis*. Wiley, New York, 1988.

[9] J. P. Boyd. *Fourier and Chebyshev Spectral Methods*. Dover, New York, 2000.

[10] R. Peyret. *Spectral Methods for Incompressible Viscous Flow*. Springer - Verlag, New York, 2002.